Anatomically-Aware, Automatic, and Fast Registration of 3D Ear Impression Models

Alexander Zouhar, Tong Fang, Gozde Unal,
Greg Slabaugh, Hui Xie
Siemens Corporate Research
Department of Intelligent Vision and Reasoning
Princeton, New Jersey
Alexander.Zouhar@Siemens.com

Fred McBagonluri
Siemens Hearing Instruments
Piscataway, New Jersey

Abstract

We present a registration framework based on feature points of anatomical 3D shapes represented in the point cloud domain. Anatomical information is utilized throughout the complete registration process. The surfaces, which in this paper are ear impression models, are considered to be similar in the way that they possess the same anatomical regions but with varying geometry. First, in a shape analysis step, features of important anatomical regions (such as canal, aperture, and concha) are extracted automatically. Next these features are used in ordinary differential equations that update rigid registration parameters between two sets of feature points. For refinement of the results, the GCP algorithm is applied. Through our experiments, we demonstrate our technique's success in surface registration through registration of key anatomical regions of human ear impressions. Furthermore, we show that the proposed method achieves higher accuracy and faster performance than the standard GCP registration algorithm.

1 Introduction

Registration of surfaces is a fundamental task with numerous applications in different fields such as computer vision and medical imaging. In general it is defined as alignment between surfaces by means of certain transformations, for instance, rotation and translation.

Given two 3D surfaces, whether from a same or a different shape class, the problem of generic registration is a difficult one usually due to large variability in the inter-shape or even intra-shape classes. Particularly, direct registration between two 3D surfaces represented as point clouds may be prone to errors due to the high dimensionality of the shape space in which the anatomic structures are represented. Extraction of useful and relevant feature points from the shapes provides a dimensionality reduction in the shape representation, and thereby reduces the noise in the problem of registration. In this paper, we present a feature-based registration framework for anatomical 3D surfaces. Surfaces are assumed to be similar in the sense of possessing anatomical regions of the same meaning but with varying geometry among objects. Our particular interest is for the registration of human ear impression models for the manufacturing of hearing aids especially between left and right ear impression of one person. In general it can be used to register any pair of human ear impression models.

The importance of development of a specific registration algorithm for this application is derived from the objective of automating the workflow with different techniques such as binaural processing - a simultaneous manipulation of left and right ear impressions which requires a robust registration between them. On the other hand, a feature-based registration is essential because during the manufacturing process that will follow the registration, parts of the surface are cut and therefore do not play as important a role in registration as other anatomical regions. This is the reason why our algorithm needs to be anatomically aware. Another concern in our application is the speed of the registration process, which will be incorporated into a rapid prototyping system. Therefore, using a limited number of feature points is necessary and very advantageous.

A typical ear impression model, also known as an ear shell, consists of approximately $30,000$ points. Included in this point set are some important anatomical landmarks such as the ear canal, aperture, concha, and cymba, as depicted in Figure 1. Please refer to [1] for a detailed explanation of these key anatomical features. The organization of the paper is as follows. In Section 4, we discuss automatic detection of feature points. In Section 5 we present the feature-based alignment using a variational approach. In Section 6, feature-based refinement for the final registration phase is described. Section 7 presents experimental results followed by the conclusions in Section 8.

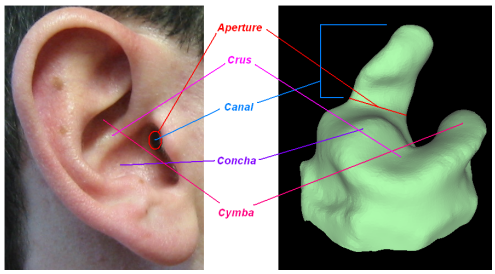

Figure 1: A human ear impression depicts important anatomical landmarks such as the ear canal, aperture, concha, and cymba on the surface.

2 Related work

As mentioned in [2] there are four approaches to representing a surface for the sake of registration: point-based, feature-based, and model-based methods as well as techniques based on global similarity. The point-based and model-based methods [3, 4, 5] do not attempt to reduce the surface representation to a more compact description; rather they use all, or a large subset of all, points [6, 7, 8, 9, 10].

By extracting feature points from a shape, one can reduce the dimensionality of shape representation and use these lower dimensional but more robust features for registration. Examples include generalized cylinders [11], super quadrics [12], geons [13], deformable regions [14], shock graphs [15], medial axes [16], and skeletons [17, 18, 19]. Our previous research shows that for the case of registration of ear impression models with 3D skeletons, sometimes reasonable results can be obtained but in general their usefulness is limited to rather rough alignments [19].

Landmarks or features extracted from the input medical data are widely used in feature-based surface registration [2, 20]. Most commonly, landmarks are identified manually, which may be tedious to determine and less repeatable than those that are automatically extracted.

Two point sets are usually registered by iteratively minimizing a global function such as the sum of squared distances between mutually closest points of two surfaces. Differences between many of these methods exist strictly at the level of the choice of distance metric and of the methods of optimally finding a match based on this metric. Besl and McKay [21] propose the well known Iterative Closest Point (ICP) method as a solution to this problem. Variants of the ICP algorithm are discussed in [22].

3 Proposed Approach

We consider anatomical regions of surfaces as landmarks and present them as sets of 3D points. After the initial feature extraction stage, correspondences between two sets of points that belong to anatomical regions of the same meaning have to be found.

Our goal is to utilize the compact information provided by a set of feature points in description of a surface to aid in the registration between two shapes. The main idea is to automatically detect feature points from key anatomical regions of the ear impression surfaces and to utilize this information throughout the complete registration process.

Particularly with regard to hearing aids, the aperture region is one of the most important features [23]. Consequently, our registration method first performs a pre-registration by rigidly aligning the aperture region of the impressions. We define an energy functional based on the L^2 distance between the apertures, derive ordinary differential equations to update the rigid registration parameters between these feature points, and minimize this energy functional in a variational framework. Upon convergence, we apply the estimated registration parameters to the entire shape to achieve a reasonable pre-alignment.

Although for this type of registration there are closed form solutions such as Horn's method [24] based on unit quaternions, we found that our iterative solution is more intuitive, and easy to use.

In order to improve the results, we perform a second refinement step using a denser set of feature points and the GCP algorithm. As in the pre-registration, this refinement step focuses on anatomic regions of the surfaces that are of special importance with respect to the similarity of two ear impressions. The final registration results are computed more quickly and have significantly higher accuracy in the canal, aperture, and concha regions than the standard GCP registration algorithm.

4 Automatic Shape Analysis

To achieve our goal of registration of ear impressions with respect to important anatomic regions such as the aperture, canal and concha, we must first detect these regions from the ear impression. The detection is automatic and is based on the analysis of scan lines that slice through the surface. During the laser scanning of an impression, the bottom of the surface is invisible, which results in an open bottom of the surface as shown in Figure 2.

From this, we detect the bottom opening of the raw impression (see Figure 2) calculating the first two principal components of the bottom contour. The bottom plane is used to find the tip of the canal (the topmost point in the vertical direction). We then perform a scan in the orientation perpendicular to the plane.

The aperture of a human ear impression is considered as a characteristic contour that connects canal and remaining impression body. In other words, it is the entrance of

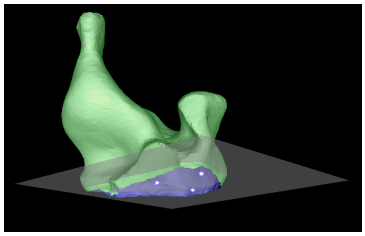

Figure 2: The bottom plane is defined by the first two principle components of the boundary points.

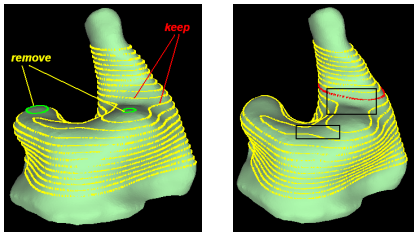

(a) (b)

Figure 3: The set of contours, shown in (a), is obtained by a vertical scan of the surface. In (b), the positions of significant changes of contour shapes are highlighted by rectangles.

the canal. An analysis of adjacent contour lines reveals a significant change of contour shape around the aperture position, and additionally in the area where the concha merges into the lower part of the surface, as shown in Figure 3(b). We use this observation to detect the aperture as described in Section 4.1. Due to the anatomical importance of the aperture feature, in the variational pre-alignment phase discussed in the next section, we use feature point set $\boldsymbol{A}$ obtained from the aperture contour as depicted in Figure 6.

4.1 Aperture detection

In Figure 3(a) a complete scan profile of an ear impression is depicted in which different colors indicate that more than one contour line exist at a particular scan level. If that is the case we want to exclude contour lines, as marked in the same figure and keep only lines along canal and lower impression part. Usually the number of contour lines at one level will not exceed a value of three. The remaining set of contour lines - the Aperture profile - is shown in Figure 3(b).

We extract the aperture profile from the complete set of vertical scan lines starting at the canal tip downwards to the bottom of a surface. If there is only one contour line at scan level i it is directly considered as part of the aperture profile. In case of more than one contour line at scan level i only the contour whose center has minimal distance to the

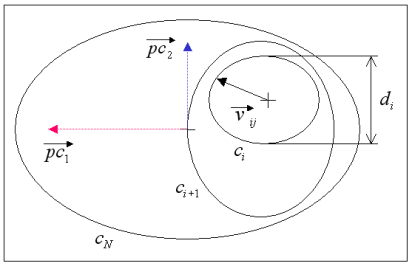

Figure 4: Calculation of the projection difference d_i for contour line c_i. Vector $\vec{\boldsymbol{v}}_{ij}$ shows how the contour point vectors are defined: from the center of the contour i to the actual contour point j.

center of the contour, which was extracted at scan level $i-1$ is inserted to the aperture profile. The observation shown in Figure 3(b) led us to use a weighted filter that assigns weights of higher importance to canal and concha area. This filter rule (1) works on the first derivative of measures calculated on each scan line contour, and helps extraction of an aperture profile function whose maximum value defines the contour index corresponding to the aperture scan line contour.

$$val_i = f_i \cdot (d_i - d_{i-1}),\ f_i = 1 - i/N,\ 2 \le i \le N \quad (1)$$

$$pos = \arg\max_i (val_i) - 1, 1 \le pos \le N - 1 \quad (2)$$

In Equation (1) N denotes the number of contour lines. Figure 4 shows a schematic top view of aperture profile contour lines. The smaller contours depict canal and concha area respectively. Points of line i are considered as vectors $\vec{v}_{ij}$ originated in the contour line center. The value d_i measures the difference between the two maximum projection values of these vectors onto the second principal component $\vec{pc}_2$ of the lowest contour line c_N. In this way one would expect that the first-order backward difference $d_i - d_{i-1}$ has its maximum value at the desired object position as highlighted with the upper black rectangle in Figure 3(b). The use of contour c_N for this purpose is justified by its consistent geometrical properties and topological relations to other object parts like canal, concha and cymba despite of the diversity among shapes.

However, our experiments show that $d_i - d_{i-1}$ alone is not robust enough to handle all cases. Especially objects with a shallow concha tend to be candidates for misclassifications. In those cases contours below the expected aperture become more favoured. As a countermeasure differences of subsequent d_i are weighted with factor f_i, which assigns in a way a higher importance to the canal region. An example output of Equation (1) is shown in Figure 5. Equation (2) determines the aperture, which is one contour position above the contour extracted with Equation (1).

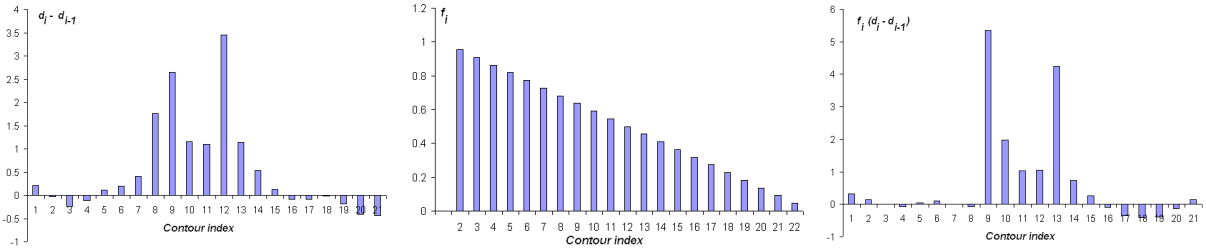

(a) (b) (c)

Figure 5: Factor f_i (b) assigns decreasing weights to the first-order backward difference $d_i - d_{i-1}$ (a) leading to the output of equation (1) shown in (c). The high peak at contour position 9 indicates that the aperture is located at position 8.

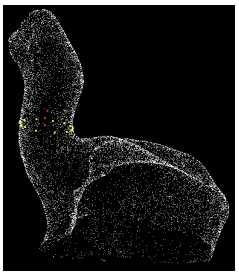

Figure 6: Reduced point set (yellow, red) $\mathbf{A}$ that will be used in the variational alignment stage.

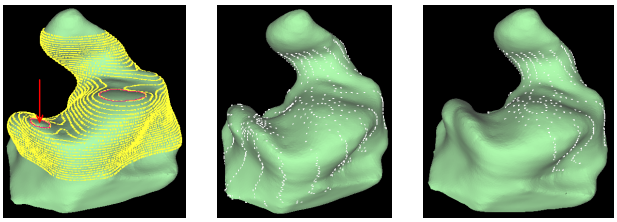

(a) (b) (c)

Figure 7: In (a), the red arrow points at the cymba region. Contours emphasized with red color indicate a topological split at that particular scan position. The second contour marked with red color refers to the concha position. In (b), we show the initial point set, and in (c), the points closer to the detected cymba point $\boldsymbol{p}_r$ have been removed.

4.2 Detection of feature points for the refinement registration

The second phase of the registration uses a denser set of points that come from canal, aperture, and concha. These are the regions to which the hearing aid device will be fit in a patient's ear. Another reason why these points are unique is the fact that left and right ear impression of one person are most similar in these regions. Accordingly, we do not want to include points from the cymba region in this step, as the cymba will be removed during the manufacturing process. To detect the cymba, we look for topological splits of the contour. These can occur both at the concha and the cymba, as shown in Figure 7 (a).

From our experiments we learn that not all impressions do have this clear topological split at the cymba position. In order to free us from the distinction between the topological change in the contour for the concha and cymba we define a reference point $\boldsymbol{p}_r$ that is definitely located in the region of the cymba:

$$\boldsymbol{p}_r = \arg\max_{\boldsymbol{p} \in P} \left\{ \frac{\boldsymbol{p} - \boldsymbol{c}}{\|\boldsymbol{p} - \boldsymbol{c}\|} \cdot \boldsymbol{x} \cdot \|\boldsymbol{p} - \boldsymbol{c}\| \right\}, \|\boldsymbol{x}\| = 1 \quad (3)$$

In equation (3) P refers to the set of all considered contour points, $\boldsymbol{c}$ is the center point of the aperture contour and $\boldsymbol{x}$ is the x-axis of the local coordinate frame, which is oriented from concha to cymba. Expression $\|\boldsymbol{p} - \boldsymbol{c}\|$ favours points of the cymba region and factor $\frac{\boldsymbol{p}-\boldsymbol{c}}{\|\boldsymbol{p}-\boldsymbol{c}\|} \cdot \boldsymbol{x}$ provides a directional constraint which gives a higher weight to the surface part where the red arrow in Figure 7 (a) points at.

We subsample the contour points to produce an initial feature point set, shown in Figure 7 (b). We avoid sampling the ear canal tip as it will be removed from the surface during detailing. Next, only those points that are closer to the aperture center than $\boldsymbol{p}_r$ are kept, resulting in a set of points $\boldsymbol{P}$ that primarily belong to canal, aperture, and concha. An example appears in Figure 7 (c), which consists of approximately 200 points, which is a very compact shape representation when compared to the original input point set with order of $30,000$ points. Point set $\boldsymbol{P}$ is used in the final refinement phase of the registration of a given object with the template object given as dense set of points.

5 Variational Registration

Given two aperture point sets $\boldsymbol{A}_1$ and $\boldsymbol{A}_2$ of 3D ear shell surfaces, we will derive a set of ordinary differential equations (ODEs) to estimate the rigid registration parameters

that transform shell 1 to shell 2. We first explain how we find the correspondences between the two feature sets $\boldsymbol{A}_1$ and $\boldsymbol{A}_2$ using anatomical information from the ear impression geometry. Then we present the variational solution to the rigid registration of two point sets.

5.1 Solving the correspondence problem

In order to find the best pair-wise correspondences between two sets of aperture points, we consider their relation with respect to the global surface. For this we define a local coordinate system (illustrated in Figure 8) in the following way: the y-direction is defined by the plane normal of the cutting plane for the vertical scan. Its orientation is assumed to be off the center of mass. The x-direction represents the main orientation of the lower surface pointing from canal to cymba and the second major direction defines the z-axis which points from canal to concha. Essentially this coordinate system is used to extract the reduced set of feature points from the aperture contour in a defined order. Figure 8 shows the local coordinate systems of a left and right ear impression model positioned in the center of the scene and the resulting important aperture points. Starting at the red point the circulation continues at the position with the yellow point and so on which defines the correspondence order. In our experiments we have used a set of 16 aperture points plus three additional points: the aperture center point and the center points of two canal contour lines above the aperture contour (Fig.6). We sample the contours in a similar fashion to produce the feature points in the refinement registration step.

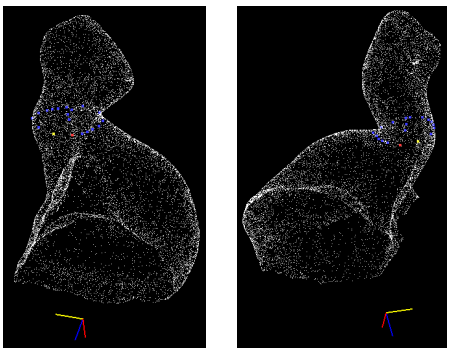

Figure 8: Shown are two 3D point clouds of a left and right hearing aid shell model from the same person together with their local coordinate systems. The red line represents the x-axis, the blue line stands for the y-axis and the yellow line for the z-axis.

5.2 Variational Optimization

We want to register two vectors of feature points, $\boldsymbol{A}_1$ and $\boldsymbol{A}_2$. That is, we want to estimate the six rigid registration parameters: three parameters for 3D translation $\boldsymbol{T}$, and three parameters for 3D rotation $\boldsymbol{R}$ which map one of the aperture vectors onto the other one. In order to write a cost functional which expresses the estimation error for the registration between the two feature vectors, first we have to find the correspondences between the aperture points. We resort to the correspondence finding algorithm mentioned above to tackle this problem.

After we obtain the information necessary to compare aperture points, we can write an energy functional, which penalizes the squared L^2 distance, and vanishes when the second feature vector $\boldsymbol{A}_2$ perfectly matches the first one $\boldsymbol{A}_1$:

$$E(\boldsymbol{R},\boldsymbol{T}) = ||\boldsymbol{A}_1 - (\boldsymbol{R}\cdot\boldsymbol{A}_2 + \boldsymbol{T})||^2 \qquad (4)$$

Representing the aperture points as a set of 3D points: $\boldsymbol{A}_1 = [\boldsymbol{X}_1, \boldsymbol{X}_2, ..., \boldsymbol{X}_n]$, and $\boldsymbol{A}_2 = [\boldsymbol{Y}_1, \boldsymbol{Y}_2, ..., \boldsymbol{Y}_n]$, where n is the number of points, we have:

$$E = \sum_{i=1}^{n} ||\boldsymbol{X}_i - (\boldsymbol{R}\boldsymbol{Y}_i + \boldsymbol{T})||^2 . \qquad (5)$$

In this equation, we use the corresponding points from the two apertures in the summation of the Euclidean distances between the points of $\boldsymbol{A}_1$ and the transformed $\boldsymbol{A}_2$. The first variation of this cost functional w.r.t. the translation parameters $T^k,\ k = 1, ..., 3$ are given by:

$$\frac{\partial T^k}{\partial t} = \sum_{i=1}^{n} < [\boldsymbol{X}_i - (\boldsymbol{R}\boldsymbol{Y}_i + \boldsymbol{T})], \frac{\partial \boldsymbol{T}}{\partial T^k} >, \qquad (6)$$

where

$$\frac{\partial \boldsymbol{T}}{\partial T^1} = \begin{pmatrix} 1 \\ 0 \\ 0 \end{pmatrix}, \quad \frac{\partial \boldsymbol{T}}{\partial T^2} = \begin{pmatrix} 0 \\ 1 \\ 0 \end{pmatrix}, \quad \frac{\partial \boldsymbol{T}}{\partial T^3} = \begin{pmatrix} 0 \\ 0 \\ 1 \end{pmatrix},$$

and $< .,. >$ denotes an inner product in 3D Euclidean space.

For defining rotation in 3D, we use exponential (a.k.a. twist) coordinates where a 3D vector $\boldsymbol{w} = (w_1, w_2, w_3)$ represents the rotation matrix, and operations can be carried easily as in the translation vector (for details see [25]). The skew symmetric matrix corresponding to $\boldsymbol{w}$ is given by

$$\hat{\boldsymbol{w}} = \begin{bmatrix} 0 & -w_3 & w_2 \\ w_3 & 0 & -w_1 \\ -w_2 & w_1 & 0 \end{bmatrix}$$

and the rotation matrix is $\boldsymbol{R} = e^{\hat{\boldsymbol{w}}}$. Then the first variation of the cost in (5) w.r.t. rotation parameters are given by:

$$\frac{\partial w^k}{\partial t} = \sum_{i=1}^{n} < [\boldsymbol{X}_i - (\boldsymbol{R}\boldsymbol{Y}_i + \boldsymbol{T})], \boldsymbol{R}\frac{\partial \hat{\boldsymbol{w}}}{\partial w^k}\boldsymbol{Y}_i >, \quad (7)$$

where

$$\frac{\partial \hat{\boldsymbol{w}}}{\partial w^1}\boldsymbol{Y}_i = \begin{pmatrix} 0 \\ -Z_i \\ Y_i \end{pmatrix}, \frac{\partial \hat{\boldsymbol{w}}}{\partial w^2}\boldsymbol{Y}_i = \begin{pmatrix} Z_i \\ 0 \\ -X_i \end{pmatrix}, \frac{\partial \hat{\boldsymbol{w}}}{\partial w^3}\boldsymbol{Y}_i = \begin{pmatrix} -Y_i \\ X_i \\ 0 \end{pmatrix}.$$

Note that as the initial condition for these ordinary differential equations, we take $T^1 = 0,\ T^2 = 0,\ T^3 = 0$, and similarly, $w_1 = 0,\ w_2 = 0,\ w_3 = 0$, which is equivalent to taking $\boldsymbol{R} = \boldsymbol{I}$ (identity matrix). Furthermore, every time $\boldsymbol{w} = (w_1, w_2, w_3)$ is updated, the new rotation matrix can be computed as

$$\boldsymbol{R} = \cos(t)\boldsymbol{I} + \sin(t)\hat{\boldsymbol{w}}_* + (1-\cos(t))\boldsymbol{w}_*\boldsymbol{w}_*^T,$$

where $t = ||\boldsymbol{w}||,\ \boldsymbol{w}_* = \frac{\boldsymbol{w}}{t}$ [25]. We use the simple gradient descent method with momentum in order to optimize the motion parameters [26].

Since the pre-alignment registers a reduced set of points, it is fast, and gives an excellent initialization for subsequent refinement. While it would be possible to adapt the variational approach to refine the registration using more points of the shells, we would again face the problem of finding corresponding points between the two surfaces. Instead, after the apertures are aligned using the variational approach, we refine the alignment by performing dense surface registration using a variant of the iterated closest point (ICP) algorithm, which does not require explicit correspondences. This refinement step is discussed in the next section.

6 Final Refinement Step in Registration

In this section we address the alignment problem of two preregistered ear impression models given as 3D dense point sets, say $\boldsymbol{P}$ and $\boldsymbol{M}$. We choose to work with the Grid Closest Point (GCP) algorithm [27], which works well in practice and is exceptionally fast. This algorithm determines the corresponding (closest) model data points $\boldsymbol{M}$ in every GCP step.

Again for a Euclidean motion with rotation matrix $\boldsymbol{R}$ and translation vector $\boldsymbol{T}$, denote the transformed points of the data set $\boldsymbol{P}$ by

$$\boldsymbol{p}_i(\boldsymbol{R}, \boldsymbol{T}) = \boldsymbol{R}\boldsymbol{p}_i + \boldsymbol{T}, 1 \leq i \leq N \tag{8}$$

Hence, we wish to minimize the sum of the squared individual distances E^i:

$$E = \sum_{i=1}^{N} E^i, \tag{9}$$

with

$$E^i = \left\| \arg\min_{\boldsymbol{m} \in \boldsymbol{M}} \|\boldsymbol{m} - \boldsymbol{p}_i(\boldsymbol{R}, \boldsymbol{T})\| - \boldsymbol{p}_i(\boldsymbol{R}, \boldsymbol{T}) \right\|^2 \tag{10}$$

Hence we find the motion $(\boldsymbol{R}, \boldsymbol{T})$ that minimizes the sum of the least N squared individual distances $E^i = d_i^2(\boldsymbol{R}, \boldsymbol{T})$ in Equation (9) by means of an algorithm based on the concept of conjugate gradients [28, 26]. We numerically solve for the derivatives of the error function (9) using finite differences.

Additionally we want to steer the registration process with information about important object regions. As discussed in Section 4, the important object regions are aperture, concha, and canal. One way to express importance is to assign weights to points depending on their position. The most promising weight function we found is a step function that rejects points not belonging to important object parts. In this way we avoid biasing the registration, and instead focus only on the canal, aperture, and concha regions to which the hearing aid will be fit.

7 Experimental results

Assessment of the required level of accuracy in registration is an application-dependent problem. It is important to realize that shapes of ear impressions can vary with respect to their similarity from almost equal up to very different. Very similar are usually a left and right ear impression from the same person. To obtain an accuracy characterization in general we focus on the overlap accuracy of three important visual landmarks namely aperture, concha and (lower) canal. We measure the registration accuracy with the root mean square value (MSE) of the sum of the distances between the two feature point sets.

We compare our framework (including feature detection and registration) with the standard GCP registration technique when applied to ear impression models. While our method uses a reduced set of important anatomical points, GCP considers all points of the surface to be registered.

Figure 9(a) shows the unregistered state of surface S_1 (yellow) and surface S_2 (blue). The feature points used for the final registration with our method and the calculation of the MSE are shown in Figures 9 (b) and 9 (c). Figure 10 depicts the alignment between S_1 and S_2 from three vantage points using our method (left). Now we repeat the experiment and register S_2 with S_1 by using only GCP with the complete dense point set of S_2. The result is presented in Figure 10 (right). A comparison of the visualizations shows that our method achieves a better overlap with respect to important object parts. After applying GCP one can see that especially the concha area is not well matched. The accurate overlap of this object part is of specific importance for binaural processing.

For both registration methods the same points as illustrated in Figure 7 (c) are used in order to calculate the MSE. Table 1 presents a comparison between the GCP registration technique and our method. We used a data set of 30 ear

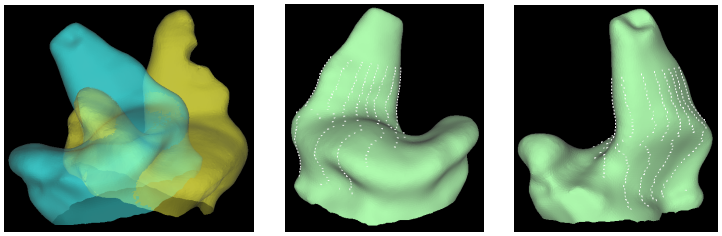

(a) (b) (c)

Figure 9: The initial position of surface S_1 (yellow) and S_2 (blue) is shown in (a). Our method uses the highlighted points shown in (b) and (c) for the final registration. The calculation of the MSE using these points allows a comparison with other registration algorithms.

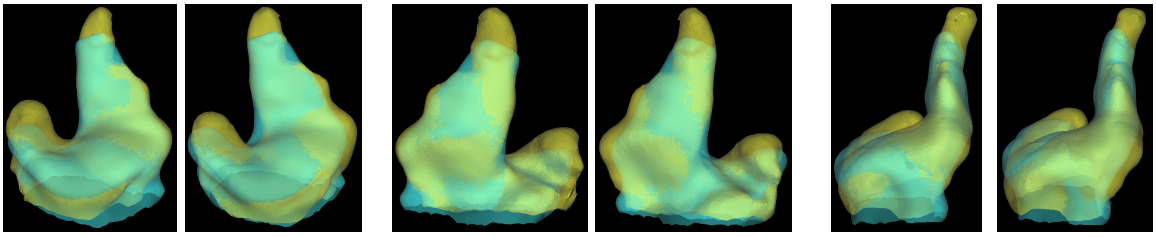

Our method (1) GCP (1) Our method (2) GCP (2) Our method (3) GCP (3)

Figure 10: Example for the registration of two ear impression models. Three pairs of figures depict the result from three different vantage points using our method (left) and GCP (right). Notice the different accuracies with respect to the concha region.

Our method		GCP	
MSE	Time (seconds)	MSE	Time (seconds)
0.31	22	1.83	180

Table 1: Comparison of our method with GCP.

impression models, and the average MSE values reported in Table 1 support the visual inspection results that our algorithm achieves a more accurate registration particularly w.r.t. important and relevant anatomical landmarks. An additional advantage as can be observed from the table is that our algorithm runs much faster than the standard GCP algorithm.

In Figure 11 we present two more examples of our method, showing the initial stage in the left column and the result after applying the registration in the right column respectively. The yellow colored surface serves as registration template. Notice the successful overlay of Canal, Concha and Aperture.

8 Summary and Conclusions

We presented a registration framework based on feature points of anatomical 3D shapes represented in the point cloud domain. Surfaces are considered as similar in the way that they possess the same anatomical regions but with varying geometry. The first step is to detect features of important anatomical regions automatically. We derived ordinary differential equations to update six registration parameters (translation and rotation) between two sets of feature points around the aperture. Applying the estimated parameters to the corresponding shapes, our algorithm achieves a fast and accurate pre-alignment. In order to refine the results the GCP algorithm is applied, with emphasis on the points of important object regions.

Our experiments reveal that compared to the standard GCP technique for surface registration in the point cloud domain, our algorithm achieves more accurate results by exploiting anatomical information throughout the complete registration process. Another beneficial property of our algorithm is that it is fast because of the limited number of points involved in the process. Although in this paper we focussed on the fast and accurate alignment of ear impression surfaces, this framework can be applied to the registration of any structures for which importance can be assigned to different regions although their detection will vary from case

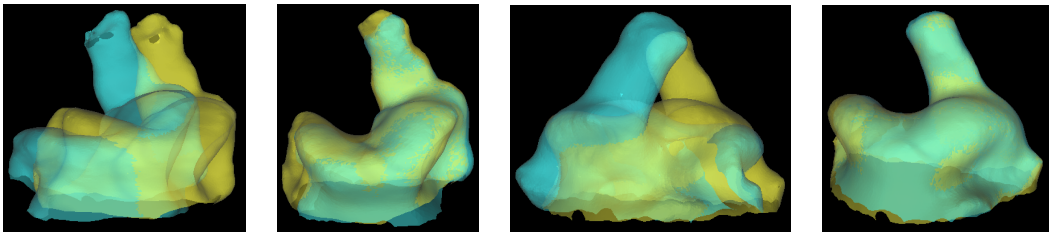

(Initial position) (Result) (Initial position) (Result)

Figure 11: Examples for the registration of two ear impression models with our method.

to case. Besides the integration of the registration framework into our current software system for binaural processing, one of our future goals is to find a more general feature detection approach in order to minimize heuristic decisions for the detection of important anatomical regions.

References

[1] Henry Gray, "Gray's anatomy of the human body," *www.bartleby.com/107/*, 1918.

[2] Michel A. Audette, Frank P. Ferrie, and Terry M. Peters, "An algorithmic overview of surface registration techniques for medical imaging," *Medical Image Analysis*, 1999.

[3] H. Chui and A. Rangarajan, "A new algorithm for non-rigid point matching," in *CVPR*, 2000, pp. 44–51.

[4] X. Huang, N. Paragios, and D. Metaxas, "Establishing local correspondences towards compact representations of anatomical structures," in *MICCAI*, 2003, pp. 926–934.

[5] N. Paragios, M. Rousson, and V. Ramesh, "Matching distance functions: A shape-to-area variational approach for global-to-local registration," in *ECCV*, 2002, pp. 775–790.

[6] B. Horn, "Extended gaussian images," *Proc. of the IEEE*, vol. 72, no. 12, pp. 1671–1686, 1984.

[7] H. Delingette, M. Hebert, and K. Ikeuchi, "Shape representation and image segmentation using deformable surfaces," *Image and vision comp.*, vol. 10, no. 3, pp. 132–144, 1992.

[8] M. Hebert H. Delingette and K. Ikeuchi, "A spherical representation for the recognition of curved objects," *ICCV*, p. 103112, 1993.

[9] D. Zhang and M. Hebert, "Harmonic maps and their applications in surface matching," *IEEE Conference on Computer Vision and Pattern Recognition*, 1999.

[10] A. E. Johnson and M. Hebert, "Using spin-images for efficient multiple model recognition in cluttered 3-d scenes," *IEEE PAMI*, vol. 21, no. 5, pp. 433449, 1999.

[11] T. Binford, "Visual perception by computer," *IEEE Conference on Systems Science and Cybernetics*, 1971.

[12] F. Solina and R. Bajcsy, "Recovery of parametric models from range images: The case for superquadrics with global deformations," *Pattern Analysis and Machine Intelligence*, vol. 12, no. 2, pp. 131–147, 1990.

[13] K. Wu and M. Levine, "Recovering parametrics geons from multiview range data," *CVPR*, p. 159166, 1994.

[14] R. Basri, L. Costa, D. Geiger, and D. Jacobs, "Determining the similarity of deformable shapes," *Vision Research*, vol. 38, pp. 23652385, 1998.

[15] K. Siddiqi, A. Shokoufandeh, S. J. Dickinson, and S. W. Zucker, "Shock graphs and shape matching," *Computer Vision*, pp. 222–229, 1998.

[16] E. Bardinet, S. F. Vidal, S. D. Arroyo, G. Malandain, and N. P. de la Blanca Capilla, "Structural object matching, technical report decsai-000303," Tech. Rep., Dept. of Computer Science and AI, University of Granada, Spain, 2000.

[17] J. Bloomenthal and C. Lim, "Skeletal methods of shape manipulation," *Shape Modeling and App.*, pp. 44–47, 1999.

[18] D. W. S. et al., "Skeleton-based modeling operations on solids," *Solid Modeling*, pp. 141–154, 1997.

[19] "Rigid Registration of 3D Shapes with Skeletons," *Siemens Corporate Research, Technical Report*, 2004.

[20] J. B. Antoine Maintz and Max A. Viergever, "A survey of medical image registration," *Medical Image Analysis*, 1998.

[21] P.J. Besl and N.D. McKay, "A method for registration of 3-d shapes," *IEEE Trans. Pattern Analysis and Machine Intelligence*, vol. 14, pp. 239–256, 1992.

[22] S. Rusinkiewicz and M. Levoy, "Efficient variants of the ICP algorithm," in *Proceedings of the Third International Conference on 3-D Digital Imaging and Modeling*, 2001.

[23] Fred McBagonluri, "E-detailing: Definitive methods 1.0," Tech. Rep., Siemens, Erlangen, 2002.

[24] B.K.P. Horn, "Closed-form solution of absolute orientation using unit quaternions," *J. of Optical Soc. of Amer.*, 2002.

[25] R.M. Murray, Z. Li, and S. Sastry, *A Mathematical Introduction to Robotic Manipulation*, CRC Press, 1994.

[26] Christopher M. Bishop, *Pattern Recognition*, Oxford University Press Inc., New York, 1995.

[27] S. M. Yamany, M. N. Ahmed, E. E. Hemayed, and A. A. Farag, "Novel surface registration using the grid closest point (GCP) transform," *ICIP '98*, vol. 3, 1998.

[28] William H. Press, Saul A. Teukolsky, William T. Vetterling, and Brian P. Flannery, *Numerical Recipes in C - The Art of Scientific Computing, Second Edition*, Cambridge University Press, Cambridge, 2002.